PAPER • OPEN ACCESS

Universal route for the emergence of exceptional points in PT-symmetric metamaterials with unfolding spectral symmetries

New Journal of Physics
The open access journal at the forefront of physics

Deutsche Physikalische Gesellschaft DPG
IOP Institute of Physics

Published in partnership with: Deutsche Physikalische Gesellschaft and the Institute of Physics

OPEN ACCESS

RECEIVED
23 February 2021

REVISED
27 May 2021

ACCEPTED FOR PUBLICATION
9 June 2021

PUBLISHED
2 July 2021

PAPER

Universal route for the emergence of exceptional points in PT-symmetric metamaterials with unfolding spectral symmetries

Yanghao Fang[1], **Tsampikos Kottos**[2] and **Ramathasan Thevamaran**[1,3,*]

[1] Department of Materials Science and Engineering, University of Wisconsin-Madison, Madison, WI 53706, United States of America
[2] Wave Transport in Complex Systems Lab, Department of Physics, Wesleyan University, Middletown, CT 06459, United States of America
[3] Department of Engineering Physics, University of Wisconsin-Madison, Madison, WI 53706, United States of America
[*] Author to whom any correspondence should be addressed.

E-mail: tkottos@wesleyan.edu and thevamaran@wisc.edu

Keywords: PT-symmetry, exceptional point, elastodynamics, metamaterial, fractal, quasiperiodic, aperiodic

Supplementary material for this article is available online

Abstract

We introduce a class of parity-time symmetric elastodynamic metamaterials (Ed-MetaMater) whose Hermitian counterpart exhibits unfolding (fractal) spectral symmetries. Our study reveals a scale-free formation of exceptional points in those Ed-MetaMaters whose density is dictated by the fractal dimension of their Hermitian spectra. We demonstrate this scale-free EP-formation in a quasi-periodic Aubry-Harper Ed-MetaMater, a geometric H-tree-fractal Ed-MetaMater, and an aperiodic Fibonacci Ed-MetaMater—each having a specific fractal spectrum—using finite element models and establish a universal route for EP-formation via a coupled mode theory model with controllable fractal spectrum. This universality may enable the rational design of novel Ed-MetaMater for hypersensitive sensing and elastic wave control.

1. Introduction

Distinct from common geometric symmetries of phononic crystals and metamaterials, the parity-time (PT)-symmetric materials [1–5] utilize hidden symmetries that are encoded in the governing dynamical equations and are consequences of judicious spatially-distributed attenuation and amplification mechanisms. The PT-symmetric systems have been shown to exhibit novel transport phenomena in various application domains such as optics [6–10], microwaves and radiofrequency waves [11–14], and acoustics [4, 15–20]. Unidirectional invisibility [17, 18], shadow-free sensing [16], asymmetric switching [4, 12], and non-reciprocal transport [21, 22] are some of those exotic wave phenomena that have been demonstrated both theoretically and experimentally. On the other hand, very few works have been focused on the implementation of PT-symmetry in the realm of elastodynamics concerning the elastic wave dynamics in solids [5, 23].

A PT-symmetric elastodynamic metamaterial (Ed-MetaMater) has recently been realized by embedding a gain and a lossy mechanical resonators in an elastic medium that facilitates coupling between them [5]. When the intensity of the equal gain and loss and/or the elastic coupling strength between the two resonators of such an Ed-MetaMater are varied, a branch-point singularity forms where the eigenvalues as well as the corresponding eigenmodes of the system coalesce. Such degeneracy is known as an exceptional point (EP) and it is the most intriguing feature of PT-symmetric systems: it signifies a transition from a parameter domain where the eigenfrequencies are real and the corresponding eigenmodes of the system respect the PT-symmetry (exact PT-symmetric phase) to a domain where the eigenfrequencies are complex conjugate pairs and the normal modes violate the PT-symmetry (broken PT-symmetric phase) [24, 25]. The

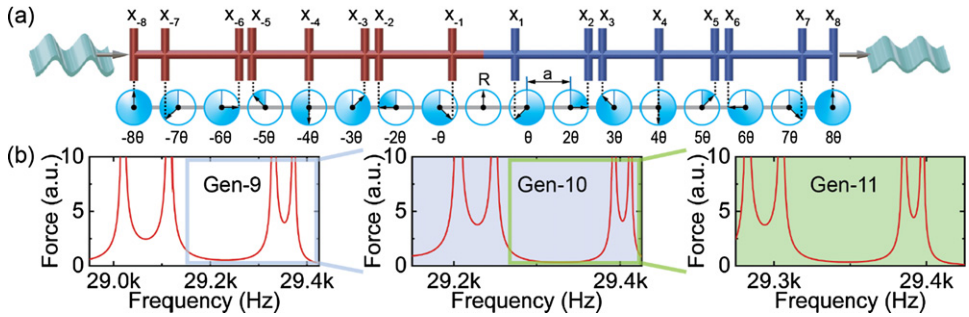

Figure 1. (a) Illustration of a generation-7 (Gen-7) Aubry-Harper Ed-MetaMater; red/blue represents energy gain/loss. For the right half (blue) of the Ed-MetaMater, 8 vertical beams (length: 6 cm; radius: 0.5 cm) are coupled by a horizontal rod with the beam positions given by $x_s = sa + R\sin(s\theta)$, where $s \in \mathrm{Z}$ is the rod index, a (5 cm) is the distance between the centers of neighboring projection circles, and R ($2\ \mathrm{cm} < a/2$) is the radius of the circle. The left half of the Ed-MetaMater (red) is a mirror reflection of the right one. The metamaterial is made of aluminum (Young's modulus: 68.9 GPa, Poisson's ratio: 0.33, density: 2700 kg m^{-3}) to which the gain/loss is introduced by structural anti-damping/damping. (b) Self-similarity of the modes as the generation is increased from Gen-9 to Gen-11.

EPs can also be realized in a more general class of non-Hermitian systems with differential loss and without any gain [26, 27]. However, in the absence of gain, the signal quality may be affected when the overall damping in the structure is very high. In the vicinity of an EP, the degenerate eigenfrequencies can be expanded in a fractional (Puiseux–Newton) power series whose importance in sensing applications has been recognized only recently [28–31]. The EP degeneracies have so far been implemented using coupled resonators in zero (e.g. pair of coupled resonators) or one-dimensional geometries (e.g. one-dimensional arrays of coupled resonators). Developing methods that allow the implementation of EPs in more complex geometries will provide exciting opportunities to engineer mechanical wave dynamics.

The quasi-periodic, aperiodic, and geometric fractal architectures offer new ways of engineering metamaterials across multiple length scales and response time scales because of their intriguing frequency spectrum demonstrating unfolding (fractal) symmetries [15, 32–36]. For example, figure 1 shows the response of an Aubry-Harper Ed-MetaMater in which the resonance modes emerge in a self-similar manner as the generation of the Ed-MetaMater is increased from 9 to 11 (figure 1(b)). The embodiment of fractality in PT-symmetric metamaterials offers the potential to create numerous EPs in a scale-free fashion similar to the scale-free nature of their fractal frequency spectra. Here, we introduce PT-symmetric Ed-MetaMaters with fractal frequency spectra and establish a universal route for the emergence of EPs in those metamaterials. We describe the mechanisms of the emerging EPs induced by the elastodynamic interactions in three classes of such PT-symmetric Ed-MetaMater with fractal spectrum—a quasi-periodic (incommensurate) Ed-MetaMater inspired by the Aubry-Harper model [37–43], a geometric fractal Ed-MetaMater made of H-shaped motifs [44], and an aperiodic Ed-MetaMater that follows Fibonacci substitutional rule [45, 46]. The universal scale-free nature of the EP formation and its connection to the fractal dimension of the frequency spectrum of the underlying Hermitian Ed-MetaMater are established using a coupled-mode-theory (CMT) modeling.

2. Method: finite element modeling

We used a commercial finite element platform, *Abaqus Simulia*, to computationally model the steady-state dynamics of the Ed-MetaMater. The material properties of aluminum (Young's modulus: 68.9 GPa, Poisson's ratio: 0.33, density: 2700 kg m^{-3}) is assumed for all components of the Ed-MetaMater which are modeled with cylindrical beam elements. The modal response convergence has been tested for different element sizes and types and twenty 3-node quadratic Timoshenko beam elements (*Abaqus Simulia*: B32) in each segment of the structure has been chosen. The P-symmetric Ed-MetaMater is harmonically excited using a prescribed axial displacement at the left end of the horizontal coupling rod generating a longitudinal wave in the rod, and the corresponding sinusoidal axial reaction force at its fixed-right-end is measured, simulating a steady-state elastic wave dynamics in the metamaterial. The PT-symmetry is created by introducing equal amount of energy amplification and attenuation at each P-symmetric part of the Ed-MetaMater, characterized by an amplification/attenuation rate. These gain/loss mechanisms have been modeled by introducing a structural anti-damping/damping coefficient in *Abaqus Simulia* with its magnitude varying from $\gamma = 0.001$ to 1. We also used another commercial finite element platform, *COMSOL Multiphysics*, to perform eigenfrequency analyses to examine the eigenmodes of EP pairs in both

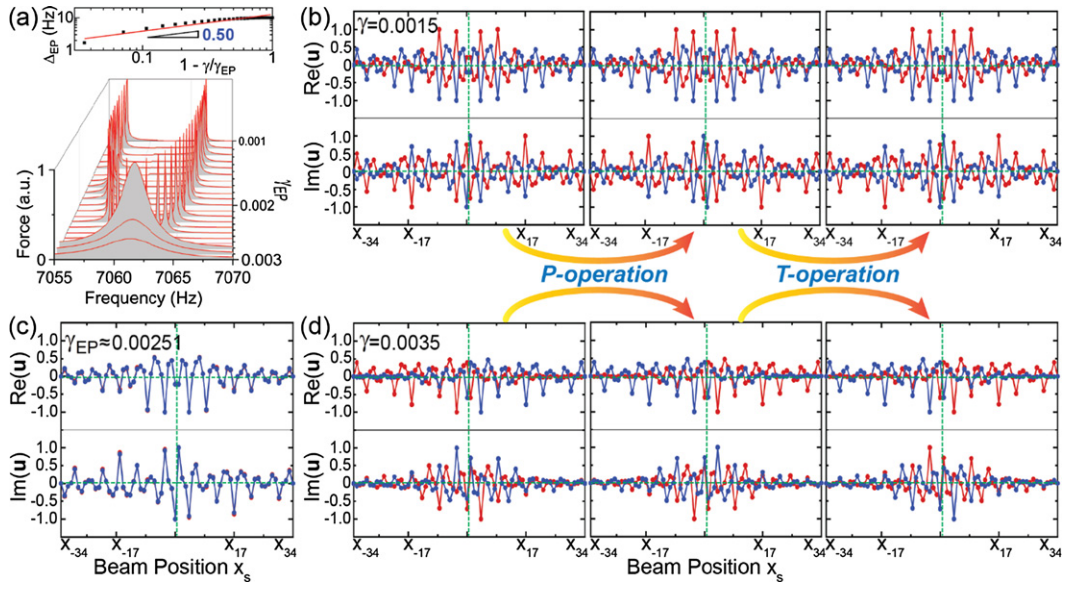

Figure 2. (a) The formation of a typical EP (inset shows a log–log plot of the frequency difference Δ_{EP} vs $1-\gamma/\gamma_{EP}$ near the EP). The red line has a slope of 0.5 shows the square-root characteristic. (b)–(d) The displacement fields $\boldsymbol{u}(x)$ of the eigenmodes corresponding to (b) the exact phase, (c) EP, and (d) broken phase (the upper and lower figures show the real and imaginary parts of the displacement field and red/blue represents mode-1/mode-2).

exact and broken phases (figures 2(b)–(d)). In this model, quadratic Timoshenko beam elements have been used and the ends of the coupling rod on either side has been fixed-constrained to respect P-symmetry. The response consistency between *Abaqus Simulia* and *COMSOL Multiphysics* has also been verified. It is noteworthy that these implicit dynamic simulations of fractal elastodynamic systems with PT-symmetry require significant computational time.

3. Results

3.1. PT-symmetric quasi-periodic Aubry-Harper Ed-MetaMater

The finite element model of the quasi-periodic Aubry-Harper Ed-MetaMater (figure 1(a)) is generated by several vertical beams (length: 6 cm; radius: 0.5 cm) coupled by a horizontal rod with the beam positions given by $x_s = sa + R\sin(s\theta)$, where $s \in Z$ is the rod index, a (5 cm) is the distance between the centers of neighboring projection circles, and R (2 cm $< a/2$) is the radius of the circle. When the projection parameter $\theta \in (0, 1)$ is an irrational number, the period of the impedance profile of the structure is incommensurate with the lattice period. To this end, we use the ratio of two adjacent numbers in a Fibonacci sequence for $\theta = p/q$, so that the impedance profile of the structure becomes commensurate with the lattice of rods with period q, defining the generation of this Ed-MetaMater (e.g. 7th generation (Gen-7) corresponds to $\theta = 5/8$, which is composed of the 6th and 7th numbers in Fibonacci sequence: 0, 1, 1, 2, 3, 5, 8, 13, …). The incommensurate limit associated with a truly quasi-periodic structure is investigated via a scaling procedure and it is reached when $q \to \infty$.

The P-symmetric ($\gamma = 0$) Aubry-Harper Ed-MetaMater is harmonically excited (0–25 kHz) using a prescribed axial displacement at the left end of the horizontal coupling rod generating a longitudinal wave in the rod, and the corresponding sinusoidal axial reaction force at its fixed-right-end is measured, simulating a steady-state elastic wave dynamics in the metamaterial. The fractal dimension D of its frequency spectra (see figure S1 in supplementary material (https://stacks.iop.org/NJP/23/063079/mmedia)) is calculated using the correlation-dimension method [47] and found to be $D = 0.83 \pm 0.02$ (see figure S2 in supplementary material) (a standard box-counting method results in the same D—albeit the correlation-dimension method converges faster to the value of D). We also find that the D of the P-symmetric Ed-MetaMater is the same as that of the corresponding Ed-MetaMater without being coupled to its mirror image. The D remains the same even in the PT-symmetric case—albeit in this case, it refers only to the real part of the frequencies. This robustness of the D of the real part of frequency spectrum against P or PT-symmetries was checked for all the systems we studied.

The PT-symmetry is created by introducing at each P-symmetric part of the Ed-MetaMater equal amount of energy gain and loss ($-/+\gamma$), characterized by an amplification/attenuation rate γ. When γ is

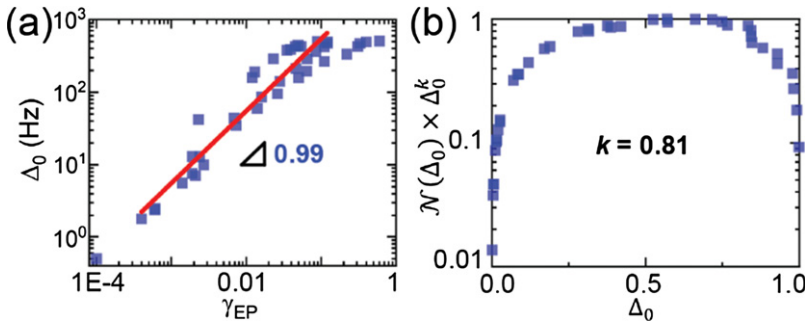

Figure 3. The EPs in PT-symmetric Gen-10 Aubry-Harper Ed-MetaMater. (a) Linear relationship between Δ_0 and γ_{EP}. (b) Integrated distribution reported as $\mathcal{N}(\Delta_0) \times \Delta_0^k$; axes normalized by their corresponding maxima.

increased, several pairs of modes interact and coalesce to form a cascade of EPs at different critical values $\{\gamma_{EP}^{(n)}\}$ and a square-root behavior typical of order-two EPs can be observed near the EP. An example of a typical EP in Gen-10 PT-symmetric Aubry-Harper Ed-MetaMater is shown in figure 2. At a critical gain/loss intensity $\gamma_{EP} = 0.00251$, the eigenvalues (figure 2(a)) and the corresponding eigenmodes (figure 2(c)) coalesce to form an EP. The square-root behavior typical of order-two EPs can be observed in the inset of figure 2(a); Δ_{EP} is the frequency difference between the corresponding mode pairs. The eigenmode components of the vector $\boldsymbol{u}(x_s)$ in (figure 2(b)–(d)) describe the displacement field of the transverse tip-deflections of the cross beams at x_s. While in our computation we evaluate the complex displacement fields, the physically relevant information is their amplitude and the phase difference between the components of the mode. We expect that for $\gamma \leqslant \gamma_{EP}$ (exact PT-symmetric phase) these eigenmodes are also eigenmodes of the PT-operator, i.e. the complex field remains invariant under the combined parity ($x_s \to x_{-s}$) and time ($i \to -i$) operations (figures 2(b) and (c)). In contrast, for $\gamma > \gamma_{EP}$ (broken PT-symmetric phase) the modes are not any more eigenmodes of the PT-operator. They are rather mapped to one another once the joint PT-operation is applied (figure 2(d)).

To further estimate the non-Hermitian perturbation strength γ that enforces an EP degeneracy for a specific pair of modes, we plot γ_{EP} vs Δ_0 for each EP found in the spectrum. Here, $\Delta_0 \equiv \Delta_{EP}|_{\gamma=0}$ is the frequency difference between the corresponding mode pairs when $\gamma = 0$. All EPs (< 25 kHz) in a Gen-10 PT-symmetric Aubry-Harper Ed-MetaMater are shown in figure 3(a). Their linear relation demonstrates the intimate relation between the initial (i.e. when $\gamma = 0$) frequency split of these two interacting modes Δ_0 and the critical gain/loss intensity γ_{EP} which coalesce those modes to form an EP. In other words, the non-Hermitian perturbation strength γ_{EP} that is needed for enforcing a degeneracy between an EP-pair must be of the same order as the frequency split of those modes in the P-symmetric Ed-MetaMater. Therefore, a statistical analysis of γ_{EP} reduces to the statistical description of these Δ_0, which are associated with the specific mode pairs that eventually form EPs. The latter is easier to evaluate numerically since it does not require a high-resolution parametric evaluation of the modes—as opposed to the precise determination of γ_{EP}.

We evaluate the probability density function (PDF) $\mathcal{P}(\Delta_0)$ of those EPs. For better statistical processing of these data, we refer to the integrated distribution $\mathcal{N}(\Delta_0) = \int_{\Delta_0}^{\infty} \mathcal{P}(x)\mathrm{d}x$ whose derivative $\mathcal{P}(\Delta_0) = -\mathrm{d}\mathcal{N}(\Delta_0)/\mathrm{d}\Delta_0$ determines the PDF of the frequency split of the EP-pairs and therefore the PDF $\mathcal{P}(\gamma_{EP})$ of the gain/loss intensity that is necessary for inducing an EP degeneracy. We find that

$$\mathcal{N}(\Delta_0) = \int_{\Delta_0}^{\infty} \mathcal{P}(x)\mathrm{d}\tilde{x}\Delta_0^{-k}, \tag{1}$$

where the best fit parameter k is found to be $k = 0.81 \approx D$. Thus, the PDF for the gain/loss intensity scales as $\mathcal{P}(\gamma_{EP}) \sim \gamma_{EP}^{-(1+D)}$, which is represented by the flat spread in $\mathcal{N}(\Delta_0) \times \Delta_0^k$ vs Δ_0 (figure 3(b)).

3.2. The PT-symmetric H-tree geometric fractal Ed-MetaMater

We investigate another class of Ed-MetaMater whose fractal spectrum is originating from a geometric fractality in configuration space [44]. The H-tree geometric fractal Ed-MetaMater is made of two identical planar components made of H-motifs (figure 4(a)). The first generation of this fractal contains two H-shaped structures—each made of three identical cylindrical beams (length: 11.6 cm, radius: 2.38 mm)—coupled by a passive (zero gain/loss) horizontal elastic rod (coupling length: 11.6 cm; length of exterior side ledges: 5.8 cm) such that they form a P-symmetric system. Each subsequent generation adds H-motifs scaled down in length by a factor of 2 (constant diameter) to each tip of the prior H-structure.

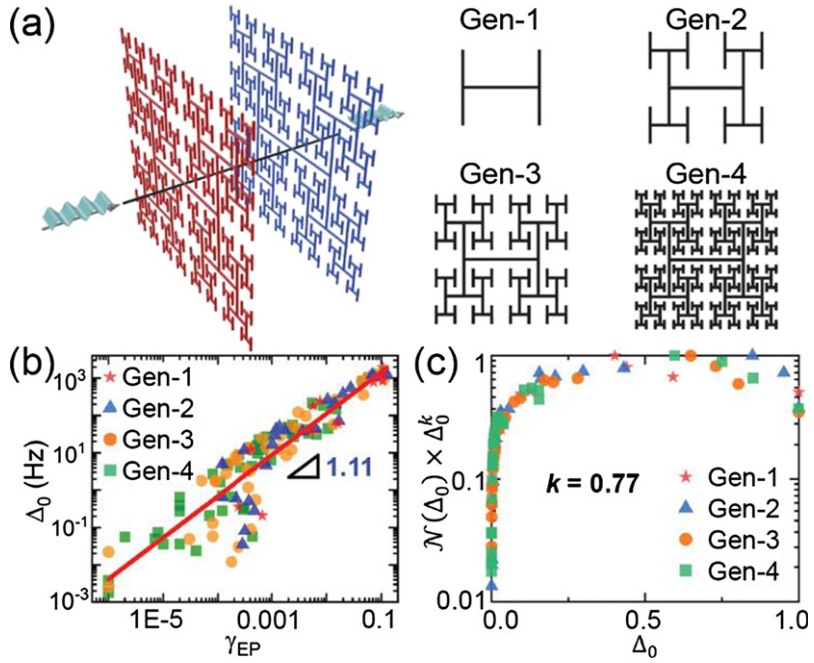

Figure 4. (a) Illustration of a Gen-4 H-tree-fractal Ed-MetaMater and first four generations of its planar component; red/blue represents energy gain/loss. The Gen-1 planar component is made of three identical cylindrical beams (length: 11.6 cm, radius: 2.38 mm). For the subsequent generations, H-motifs are scaled down in length by a factor of 2 (constant diameter) and added to each tip of the prior H-structure. Two identical planar components are then coupled by a passive (zero gain/loss) horizontal elastic rod (coupling length: 11.6 cm; length of exterior side ledges: 5.8 cm) to form a P-symmetric H-tree-fractal Ed-MetaMater. The metamaterial is made of aluminum (Young's modulus: 68.9 GPa, Poisson's ratio: 0.33, density: 2700 kg m^{-3}) to which the gain/loss is introduced by structural anti-damping/damping. (b) Linear relationship between Δ_0 and γ_{EP}. (c) Integrated distribution reported as $\mathcal{N}(\Delta_0) \times \Delta_0^k$; axes are normalized by their corresponding maxima.

The analysis of the correlation-dimension of the frequency spectrum indicates that its D converges to 0.80 (see figure S3 in supplementary material).

As previously, the PT-symmetry is created by introducing equal gain/loss ($\gamma = 0.001$–1) to the left and right planar components (figure 4(a)). The P-symmetric H-tree-fractal Ed-MetaMater is harmonically excited (0–50 kHz) using a prescribed axial displacement at the left end of the horizontal coupling rod generating a longitudinal wave in the rod, and the corresponding sinusoidal axial reaction force at its fixed-right-end is measured, simulating a steady-state elastic wave dynamics in the metamaterial (see figure S4 in supplementary material). When γ is increased, similar to Aubry-Harper Ed-MetaMater, all four generations of the PT-symmetric H-tree-fractal Ed-MetaMater show the emergence of numerous EPs at $\left\{\gamma_{EP}^{(n)}\right\}$ which are proportional to the Δ_0 associated with those specific EP-pairs (figure 4(b)). We evaluated the $\mathcal{N}(\Delta_0)$ which allows estimating the PDF $\mathcal{P}(\gamma_{EP})$ for the critical gain/loss intensity γ_{EP}. Figure 4(c) shows the integrated distribution by the variable $\mathcal{N}(\Delta_0) \times \Delta_0^k$ as a function of Δ_0. We find that for $k = 0.77 \approx D$, the data demonstrate a flat spread, leading to the conclusion that $\mathcal{P}(\gamma_{EP}) \sim \gamma_{EP}^{-(1+D)}$. This finding again demonstrates the intimate relation between the emerging EPs and the fractality of the metamaterial's spectrum.

3.3. The PT-symmetric aperiodic Fibonacci Ed-MetaMater

To further verify the universal nature of equation (1) we studied another class of Ed-MetaMater with unfolding spectral symmetries—an aperiodic system based on Fibonacci substitutional rule (figure 5(a), details in supplementary material). It is created by equally spaced (3 cm) vertical beams (lengths of A: 8 cm, B: 6 cm; radius: 0.5 cm) organized based on Fibonacci substitutional rule (further details in supplementary material) that are coupled by a horizontal rod (radius: 0.5 cm; exterior ledges: 3 cm) and then mirrored to form a P-symmetric system. The system is harmonically excited (0–50 kHz) using a prescribed axial displacement at the left end of the horizontal coupling rod generating a longitudinal wave in the rod, and the corresponding sinusoidal axial reaction force at its fixed-right-end is measured, simulating a steady-state elastic wave dynamics in the metamaterial (see figure S5 in supplementary material). The correlation-dimension analysis indicates that the frequency spectrum of this system is characterized by $D = 0.80$ (see figure S6 in supplementary material). The relation between Δ_0 and γ_{EP} is found to be linear

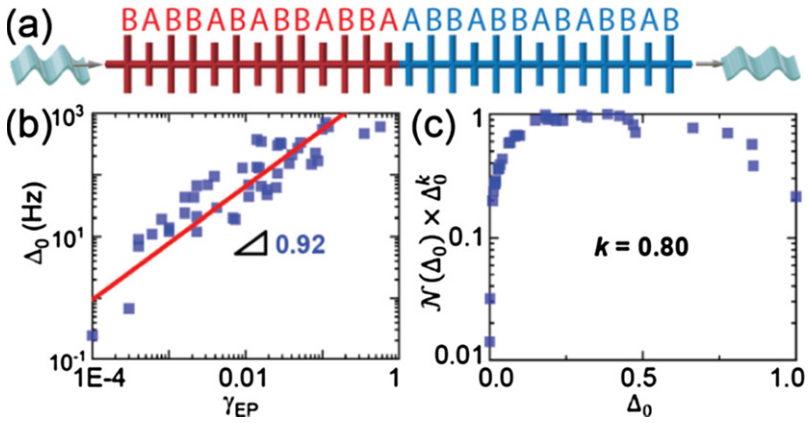

Figure 5. (a) Illustration of a Gen-7 Fibonacci Ed-MetaMater; red/blue represents energy gain/loss. The right half (blue) of the Ed-MetaMater is made by 13 equally spaced (3 cm) vertical beams (lengths of A: 8 cm, B: 6 cm; radius: 0.5 cm), the number and organization of those beams are based on Fibonacci substitutional rule (see further details in supplementary material). The left half of the Ed-MetaMater (red) is a mirror reflection of the right one. The metamaterial is made of aluminum (Young's modulus: 68.9 GPa, Poisson's ratio: 0.33, density: 2700 kg m^{-3}) to which the gain/loss is introduced by structural anti-damping/damping. (b) Linear relationship between Δ_0 and γ_{EP}. (c) Integrated distribution reported as $\mathcal{N}(\Delta_0) \times \Delta_0^k$; axes are normalized by their corresponding maxima.

again (figure 5(b)). The $\mathcal{N}(\Delta_0) \times \Delta_0^k$ vs Δ_0 demonstrates a flat spread with $k = 0.80 \approx D$ (figure 5(c)), concluding that $\mathcal{P}(\gamma_{EP}) \sim \gamma_{EP}^{-(1+D)}$.

3.4. A universal mathematical model for PT-symmetric fractal metamaterials

The intimate relation between $\mathcal{P}(\gamma_{EP})$ and the spectral fractal dimension of an Ed-MetaMater at $\gamma = 0$ implies the existence of an underlying universal route for the creation of EPs in systems with fractal spectrum. To this end, we develop a CMT-based model that utilizes on-site resonant modes that follow an aperiodic Fibonacci substitutional rule (details in figure 6(a) and supplementary material). The CMT Fibonacci model is described by the Hamiltonian:

$$H = \sum_n |n\rangle V_n \langle n| + \sum_n |n+1\rangle\langle n| + \text{c.c.}, \tag{2}$$

where the coupled resonant frequencies V_n take only two values $\pm V$ arranged in a Fibonacci sequence and $\{|n\rangle\}$ is the local mode basis. This system is known to have a Cantor-set spectrum with zero Lebesgue measure for all $V > 0$ [48]. A benefit of the Fibonacci CMT modeling is that its spectral fractal dimension D can be tuned by varying on-site resonance of the model, V, thus giving us the possibility to scrutinize the relation $\mathcal{P}(\gamma_{EP}) \sim \gamma_{EP}^{-(1+D)}$ for a variety of spectral fractal dimensions. It turns out that the PDF of the nearest level spacing $s_n \equiv \omega_{n+1} - \omega_n$ of such family of systems follows a scale-free distribution whose power-law behavior is dictated by the fractality of the spectrum, i.e. $\mathcal{P}(s) \sim s^{-(1+D)}$ [49–51]. This power law is a signature of level clustering and it is distinct from the PDF $\mathcal{P}(s)$ of chaotic or integrable systems [52, 53]. We point out that the realization of this class of systems is not confined only to aperiodic systems like the Fibonacci chain model in equation (2), but also applicable to quasi-periodic systems with metal-insulator transition at some critical value of the on-site resonance (e.g. the Aubry-Harper model) [34, 54, 55], or wave systems with a chaotic classical limit as the kicked Harper model [53]. Therefore, our CMT model represents a typical example of a whole class of systems with fractal spectrum.

The P-symmetric Fibonacci model is implemented by coupling the Hamiltonian of equation (2) with its mirror image. The corresponding effective CMT Hamiltonian takes the form:

$$H_P = \left(\sum_{n=-N}^{-1} |n\rangle V_n \langle n| + \sum_{n=-N}^{-2} |n+1\rangle\langle n| + \text{c.c.}\right) + \left(\sum_{n=1}^{N} |n\rangle \bar{V}_n \langle n| + \sum_{n=1}^{N-1} |n+1\rangle\langle n| + \text{c.c.}\right) + \left(|1\rangle\langle -1| + \text{c.c.}\right), \tag{3}$$

where $\{\overline{V}_n\}$ is the mirror-symmetric Fibonacci sequence of $\{V_n\}$ and t describes the coupling between two Fibonacci chains. We found that the P-symmetric variant has a fractal frequency spectrum with the same D as the one of the systems of equation (2). Finally, a PT-symmetric CMT model H_{PT} is implemented by introducing uniform gain/loss to the left/right portions of the system in equation (3), i.e. $V_n \to V_n - i\gamma$ and $\overline{V}_n \to \overline{V}_n + i\gamma$. Because of the simplicity in its structure, this model allows reaching higher generations for

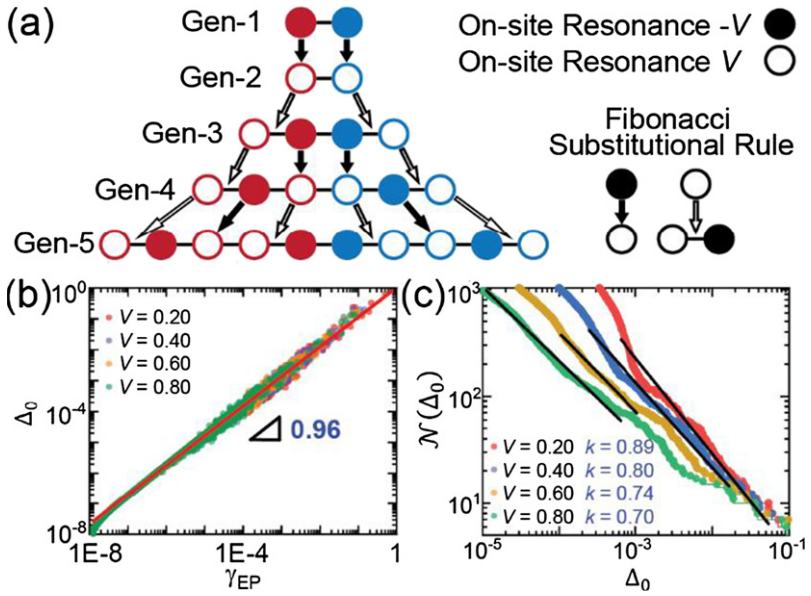

Figure 6. (a) Illustration of the first five generations of the CMT-based mathematical model with on-site resonances that follow the Fibonacci substitutional rule; red/blue represents energy gain/loss. (b) The linear relation between Δ_0 and γ_{EP}. (c) Integrated distribution $\mathcal{N}(\Delta_0)$ as functions of Δ_0 in Gen-17 Fibonacci CMT model.

more accurate numerical analyses compared to the computationally costly finite element models in previous three examples.

Consider the parametric evolution of frequencies of the P-symmetric model as the coupling constant t that connects the two Fibonacci sub-systems increases. For $t = 0$, we have two replicas of the same Fibonacci chain in equation (2) and, therefore, the spectrum consists of pairs of degenerate modes. As the coupling t increases, the degeneracy is lifted $\omega_n^{\pm} = \omega_n \pm t$. Simple degenerate perturbation theory with respect to t indicates that the new eigenstates are a linear symmetric/antisymmetric combination of the eigenstates of the Fibonacci Hamiltonian in equation (2). The above perturbative framework is applicable as long as the t is smaller than the distance between nearby frequencies $s_n = \omega_{n+1} - \omega_n$ of the uncoupled Hamiltonian H in equation (2). The frequency clustering occurring for fractal spectra, however, enforces a rapid breakdown of the perturbation theory, even for infinitesimal t. Nevertheless, the eigenstates of the Hamiltonian $H_P(t)$ are still eigenfunctions of the P-symmetric operator and therefore are symmetric or anti-symmetric with respect to the mirror axis of the total chain. The frequency spacing of nearby levels, however, is not dictated by t but the fractal nature of the spectrum.

We treat the inclusion of a small non-Hermitian element $\pm\gamma$ perturbatively. In this case the total Hamiltonian H_{PT} can be written as $H_{PT} = H_P(t) + i\gamma\Gamma$ where the $2N \times 2N$ perturbation matrix Γ has elements $\Gamma_{nm} = \delta_{nm}$ for $n \leqslant -1$ and $\Gamma_{nm} = -\delta_{nm}$ for $n \geqslant 1$. Finite γ leads to level shifts proportional to γ^2 since the first-order correction vanishes due to the P-symmetry of the corresponding unperturbed eigenmodes of $H_P(t)$. For $\gamma = \gamma_{EP} \simeq s = \Delta_0$, the perturbation theory breaks down, signaling level crossing and the appearance of pairs of complex frequencies. It is still intriguing the fact that the non-Hermitian perturbation operator $i\gamma\Gamma$ couples the nearby levels of $H_p(t)$ in the case of fractal spectrum where the validity of level spacing, and therefore of perturbation theory, is 'blurred'—specifically in the thermodynamic $N \to \infty$ limit. Nevertheless, our detailed numerical investigations confirmed the linear relation $\gamma_{EP} \sim \Delta_0$ for a variety of V-values and find that the linear relation holds with a good approximation in all cases (figure 6(b)). In case of finite system sizes N, some frequency differences Δ_0 are still dictated by t, though their weight goes to zero at the thermodynamic limit $N \to \infty$. The above analysis allows us to associate the PDF of the gain/loss intensity that results in EP degeneracy with the distribution of level spacings, leading to the conclusion that $\mathcal{P}(\gamma_{EP}) \sim \gamma_{EP}^{-(1+D)}$. We tested the validity of the above arguments numerically using the Fibonacci CMT model for a variety of potentials V and corresponding fractal dimensions $D(V)$ and in all cases we find an excellent agreement with the above theoretical results (figure 6(c)).

The figure 7 comprehensively presents the relationship between the spectral fractal dimensions of all aforementioned P-symmetric systems and the power exponents corresponding to the EPs in the PT-symmetric Fibonacci CMT model with different on-site resonances (indicated by circles; further details see figures S7 and S8 in supplementary material), the PT-symmetric Aubry-Harper Ed-MetaMater (blue

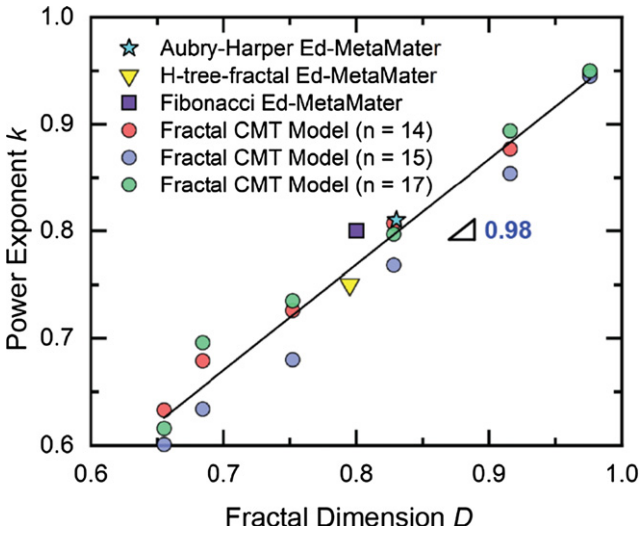

Figure 7. The universal relations between the best-fit power exponents k of the integrated distribution $\mathcal{N}(\Delta_0) \sim 1/\Delta_0^k$ and the spectral fractal dimensions D of various fractal metamaterials.

star), the PT-symmetric H-tree-fractal Ed-MetaMater (yellow triangle), and the PT-symmetric Fibonacci Ed-MetaMater (purple square). The universality in the relations between the emergence of EPs in these metamaterials and the fractality of their initial spectra is evident in figure 7. The linear fit (black line) with a slope ∼1 signifies the universality of this equality relationship, i.e., the power-law exponent describing a scale-free PDF $\mathcal{P}(\gamma_{\mathrm{EP}}) \sim \gamma_{\mathrm{EP}}^{-(1+D)}$ in a PT-symmetric Ed-MetaMater with unfolding spectral symmetries can directly be obtained from its spectral fractal dimension D. This enables a universal route for effectively predicting the emergence of EPs by the initial spectrum itself.

The linear relation found between the critical gain/loss required for creating EPs and the initial split between the mode pairs that coalesce, shows that the high-signal-quality hypersensitive sensors that exploit EPs in PT-symmetric metamaterials can be engineered by appropriate interacting mode pairs that facilitate experimentally realizable low gain/loss. Such systems can be realized via active materials, for example by using piezoelectric elements embedded in the crossbeams that are controlled by non-Foster circuits to provide balanced gain/loss [56] or in combination with passive materials with highly tunable loss [57]. Gain in ultrasonic frequency regime can also be achieved through electroacoustic amplification via phonon-electron interaction in piezoelectric semiconductor [58–60]. The classical noise in Ed-MetaMater (in contrast to quantum noise) may not be a significant concern towards achieving high signal-to-noise ratio as it has been indicated by recent studies on non-Foster circuits [61] that the noise is in same level as in typical diabolic degeneracies.

4. Conclusions

In summary, we designed three PT-symmetric metamaterials with fractal frequency spectrum—a quasi-periodic Aubry-Harper Ed-MetaMater, an H-tree geometric fractal Ed-MetaMater, and an aperiodic Fibonacci Ed-MetaMater—and investigated them using steady-state dynamic finite element approach. The scale-free emergence of numerous EPs is seen in all metamaterials, showing an intimate relation between the scale-free distribution of critical gain/loss intensities and the spectral fractal dimension of the corresponding Hermitian spectra. Particularly, the linear relation we found between the critical gain/loss required for creating EPs and the initial split between the mode pairs that coalesce, shows that the high-signal-quality hypersensitive sensors that exploit EPs in PT-symmetric metamaterials can be engineered by appropriate interacting mode pairs that facilitate experimentally realizable low gain/loss.

We further verified the findings from the specific classes of quasi-periodic, fractal, and aperiodic metamaterials and generalized them to a universal law using a CMT-based PT-symmetric fractal mathematical model. The universal relations among the creation of EPs, the scale-free probability distribution of critical gain/loss intensity, and the fractal dimension of the underlying Hermitian spectrum in these PT-symmetric Ed-MetaMater provide a powerful and convenient tool for predicting the emergence of EPs. Our findings are applicable beyond the elastodynamic realm to PT-symmetric metamaterials in acoustic, optical, microwave, and radiofrequency domains as well. We expect that our detailed numerical

results will motivate further mathematical investigations on the interplay of PT-symmetry and the systems with unfolding spectral symmetries.

Acknowledgments

We acknowledge the support from the Dynamics, Controls, and System Dynamics (DCSD) Program of the National Science Foundation (NSF) under the awards CMMI-1925530 (RT, YF) and CMMI-1925543 (TK). We also acknowledge the partial support provided by the University of Wisconsin-Madison, Office of the Vice Chancellor for Research and Graduate Education with funding from the Wisconsin Alumni Research Foundation.

Data availability statement

All data that support the findings of this study are included within the article (and any supplementary files).

ORCID iDs

Yanghao Fang https://orcid.org/0000-0003-1585-5805
Tsampikos Kottos https://orcid.org/0000-0001-6769-5984
Ramathasan Thevamaran https://orcid.org/0000-0001-5058-6167

References

[1] Bender C M and Boettcher S 1998 Real spectra in non-Hermitian Hamiltonians having PT symmetry *Phys. Rev. Lett.* **80** 5243–6
[2] El-Ganainy R, Makris K G, Khajavikhan M, Musslimani Z H, Rotter S and Christodoulides D N 2018 Non-Hermitian physics and PT symmetry *Nat. Phys.* **14** 11–9
[3] Kottos T and Aceves A B 2016 Synthetic Structures with Parity-Time Symmetry *Contemporary Optoelectronics: Materials, Metamaterials and Device Applications* ed O Shulika and I Sukhoivanov (Dordrecht: Springer) pp 147–62
[4] Thevamaran R, Branscomb R M, Makri E, Anzel P, Christodoulides D, Kottos T and Thomas E L 2019 Asymmetric acoustic energy transport in non-Hermitian metamaterials *J. Acoust. Soc. Am.* **146** 863–72
[5] Domínguez-Rocha V, Thevamaran R, Ellis F M and Kottos T 2020 Environmentally induced exceptional points in elastodynamics *Phys. Rev. Appl.* **13** 014060
[6] Musslimani Z H, Makris K G, El-Ganainy R and Christodoulides D N 2008 Optical solitons in PT periodic potentials *Phys. Rev. Lett.* **100** 030402
[7] Makris K G, El-Ganainy R, Christodoulides D N and Musslimani Z H 2008 Beam dynamics in PT symmetric optical lattices *Phys. Rev. Lett.* **100** 103904
[8] El-Ganainy R, Makris K G, Christodoulides D N and Musslimani Z H 2007 Theory of coupled optical PT-symmetric structures *Opt. Lett.* **32** 2632
[9] Hodaei H, Hassan A U, Wittek S, Garcia-Gracia H, El-Ganainy R, Christodoulides D N and Khajavikhan M 2017 Enhanced sensitivity at higher-order exceptional points *Nature* **548** 187–91
[10] Peng B *et al* 2014 Parity-time-symmetric whispering-gallery microcavities *Nat. Phys.* **10** 394–8
[11] Bittner S, Dietz B, Günther U, Harney H L, Miski-Oglu M, Richter A and Schäfer F 2012 PT symmetry and spontaneous symmetry breaking in a microwave billiard *Phys. Rev. Lett.* **108** 024101
[12] Doppler J *et al* 2016 Dynamically encircling an exceptional point for asymmetric mode switching *Nature* **537** 76–9
[13] Chitsazi M, Li H, Ellis F M and Kottos T 2017 Experimental realization of Floquet PT-symmetric systems *Phys. Rev. Lett.* **119** 093901
[14] Assawaworrarit S, Yu X and Fan S 2017 Robust wireless power transfer using a nonlinear parity-time-symmetric circuit *Nature* **546** 387–90
[15] Shi C, Dubois M, Chen Y, Cheng L, Ramezani H, Wang Y and Zhang X 2016 Accessing the exceptional points of parity-time symmetric acoustics *Nat. Commun.* **7** 11110
[16] Fleury R, Sounas D and Alù A 2015 An invisible acoustic sensor based on parity-time symmetry *Nat. Commun.* **6** 5905
[17] Zhu X, Ramezani H, Shi C, Zhu J and Zhang X 2014 PT-symmetric acoustics *Phys. Rev.* X **4** 031042
[18] Aurégan Y and Pagneux V 2017 PT-symmetric scattering in flow duct acoustics *Phys. Rev. Lett.* **118** 174301
[19] Achilleos V, Theocharis G, Richoux O and Pagneux V 2017 Non-Hermitian acoustic metamaterials: role of exceptional points in sound absorption *Phys. Rev.* B **95** 144303
[20] Ding K, Ma G, Xiao M, Zhang Z Q and Chan C T 2016 Emergence, coalescence, and topological properties of multiple exceptional points and their experimental realization *Phys. Rev.* X **6** 021007
[21] Popa B-I and Cummer S A 2014 Non-reciprocal and highly nonlinear active acoustic metamaterials *Nat. Commun.* **5** 3398
[22] Nassar H, Xu X C, Norris A N and Huang G L 2017 Modulated phononic crystals: non-reciprocal wave propagation and Willis materials *J. Mech. Phys. Solids* **101** 10–29
[23] Shmuel G and Moiseyev N 2020 Linking scalar elastodynamics and non-Hermitian quantum mechanics *Phys. Rev. Appl.* **13** 024074
[24] Bender C M 2005 Introduction to PT-symmetric quantum theory *Contemp. Phys.* **46** 277–92
[25] Moiseyev N 2011 *Non-Hermitian Quantum Mechanics* vol 9780521889 (Cambridge: Cambridge University Press)
[26] Bender C M 2018 *PT Symmetry: In Quantum and Classical Physics* (Scientific: World Scientific)
[27] Yin X and Zhang X 2013 Unidirectional light propagation at exceptional points *Nat. Mater.* **12** 175–7

[28] Wiersig J 2014 Enhancing the sensitivity of frequency and energy splitting detection by using exceptional points: application to microcavity sensors for single-particle detection *Phys. Rev. Lett.* **112** 203901
[29] Hokmabadi M P, Schumer A, Christodoulides D N and Khajavikhan M 2019 Non-Hermitian ring laser gyroscopes with enhanced Sagnac sensitivity *Nature* **576** 70–4
[30] Lai Y-H, Lu Y-K, Suh M-G, Yuan Z and Vahala K 2019 Observation of the exceptional-point-enhanced Sagnac effect *Nature* **576** 65–9
[31] Chen W, Kaya Özdemir Ş, Zhao G, Wiersig J and Yang L 2017 Exceptional points enhance sensing in an optical microcavity *Nature* **548** 192–6
[32] Demmie P N and Ostoja-Starzewski M 2011 Waves in fractal media *J. Elast.* **104** 187–204
[33] Segev M, Soljačić M and Dudley J M 2012 Fractal optics and beyond *Nat. Photon.* **6** 209–10
[34] Martínez A J, Porter M A and Kevrekidis P G 2018 Quasiperiodic granular chains and Hofstadter butterflies *Phil. Trans. R. Soc.* A **376** 20170139
[35] Naumis G G and López-Rodríguez F J 2008 The electronic spectrum of a quasiperiodic potential: from the Hofstadter butterfly to the Fibonacci chain *Physica* B **403** 1755–62
[36] Kohmoto M, Sutherland B and Tang C 1987 Critical wave functions and a Cantor-set spectrum of a one-dimensional quasicrystal model *Phys. Rev.* B **35** 1020–33
[37] Apigo D J, Qian K, Prodan C and Prodan E 2018 Topological edge modes by smart patterning *Phys. Rev. Mater.* **2** 124203
[38] Xia Y, Erturk A and Ruzzene M 2020 Topological edge states in quasiperiodic locally resonant metastructures *Phys. Rev. Appl.* **13** 014023
[39] Ni X, Chen K, Weiner M, Apigo D J, Prodan C, Alù A, Prodan E and Khanikaev A B 2019 Observation of Hofstadter butterfly and topological edge states in reconfigurable quasi-periodic acoustic crystals *Commun. Phys.* **2** 55
[40] Pal R K, Rosa M I N and Ruzzene M 2019 Topological bands and localized vibration modes in quasiperiodic beams *New J. Phys.* **21** 093017
[41] Aubry S and André G 1980 Analyticity breaking and Anderson localization in incommensurate lattices *Ann. Isr. Phys. Soc.* **3** 18 https://zbmath.org/0943.82510
[42] Yuce C 2014 PT symmetric Aubry-Andre model *Phys. Lett.* A **378** 2024–8
[43] Kuhl U and Stöckmann H-J 1998 Microwave realization of the Hofstadter butterfly *Phys. Rev. Lett.* **80** 3232–5
[44] Hou B, Xie H, Wen W and Sheng P 2008 Three-dimensional metallic fractals and their photonic crystal characteristics *Phys. Rev.* B **77** 125113
[45] Steurer W and Sutter-Widmer D 2007 Photonic and phononic quasicrystals *J. Phys. D: Appl. Phys.* **40** R229–47
[46] Maciá E 2006 The role of aperiodic order in science and technology *Rep. Prog. Phys.* **69** 397–441
[47] Strogatz S H 1994 *Nonlinear Dynamics and Chaos: With Applications to Physics, Biology, Chemistry, and engineering* (Reading, MA: Perseus Books)
[48] Sütö A 1989 Singular continuous spectrum on a cantor set of zero Lebesgue measure for the Fibonacci Hamiltonian *J. Stat. Phys.* **56** 525–31
[49] Geisel T, Ketzmerick R and Petschel G 1991 New class of level statistics in quantum systems with unbounded diffusion *Phys. Rev. Lett.* **66** 1651–4
[50] Geisel T, Ketzmerick R and Petschel G 1995 *Unbounded Quantum Diffusion and Fractal Spectra Quantum Chaos* ed G Casati and B Chirikov (Cambridge: Cambridge University Press) pp 633–60
[51] Piéchon F, Benakli M and Jagannathan A 1995 Analytical results for scaling properties of the spectrum of the Fibonacci chain *Phys. Rev. Lett.* **74** 5248–51
[52] Porter C E 1965 *Statistical Theories of Spectra: Fluctuations* (New York: Academic)
[53] Stöckmann H-J 1999 *Quantum Chaos: An Introduction* (Cambridge: Cambridge University Press)
[54] Aulbach C, Wobst A, Ingold G-L, Hänggi P and Varga I 2004 Phase-space visualization of a metal-insulator transition *New J. Phys.* **6** 70
[55] Lahini Y, Pugatch R, Pozzi F, Sorel M, Morandotti R, Davidson N and Silberberg Y 2009 Observation of a localization transition in quasiperiodic photonic lattices *Phys. Rev. Lett.* **103** 013901
[56] Schindler J, Lin Z, Lee J M, Ramezani H, Ellis F M and Kottos T 2012 PT-symmetric electronics *J. Phys. A: Math. Theor.* **45** 444029
[57] Murgado D and Thevamaran R 2020 Independent control of dynamic material properties by exploiting structural hierarchy and intrinsic structural gradients *Mater. Today Commun.* **23** 100865
[58] Hutson A R, McFee J H and White D L 1961 Ultrasonic amplification in CDS *Phys. Rev. Lett.* **7** 237–9
[59] Gokhale V J and Rais-Zadeh M 2014 Phonon-electron interactions in piezoelectric semiconductor bulk acoustic wave resonators *Sci. Rep.* **4** 5617
[60] Christensen J, Willatzen M, Velasco V R and Lu M H 2016 Parity-time synthetic phononic media *Phys. Rev. Lett.* **116** 207601
[61] Xiao Z, Li H, Kottos T and Alù A 2019 Enhanced sensing and nondegraded thermal noise performance based on PT-symmetric electronic circuits with a sixth-order exceptional point *Phys. Rev. Lett.* **123** 213901